

**PREDICTION OF DOXYCYCLINE REMOVAL BY PHOTO-FENTON PROCESS
USING AN ARTIFICIAL NEURAL NETWORK - MULTILAYER PERCEPTRON
MODEL**

Nabila Boucherit^{1*}, Salah Hanini¹, Abdellah Ibrir², Maamar Laidi¹, Mohamed
Roubhie Fissa¹

¹ *Biomaterials and Transport Phenomena Laboratory (LBMPT), Yahia Fares University,
Medea (26000), Algeria.*

² *Materials and Environment Laboratory (LME), Faculty of Technology, Yahia Fares
University, Medea (26000), Algeria.*

<https://doi.org/10.2298/CICEQ230824009B>

Received 24.8.2023.

Revised 25.1.2024.

Accepted 9.3.2024.

*corresponding author: Nabila Boucherit, E mail: na_boucherit@yahoo.fr, Tel/Fax: +213 25594552.

Abstract. This paper presents a study on the effectiveness of the Photo-Fenton Process (PF) for removing the doxycycline hyclate (DXC) antibiotic. The experiment showed that the best removal efficiency was achieved (79%) at pH 3 for 2.5 mg/L of DXC, 76.53 mg/L of H₂O₂, and 86.8 mg/L of Fe²⁺. The degradation mechanism of DXC by hydroxyl radicals was confirmed by FTIR and HPLC. To model the oxidation reaction of DXC by PF, an multilayer perceptron (MLP) based optimized artificial neural network (OANN) was used, taking into account experimental data such as pH and initial concentrations of DXC, H₂O₂, and Fe²⁺. The OANN predicted removal efficiency results were in close agreement with experimental results, with an RMSE of 0.0661 and an R² value of 0.99998. The sensitivity analysis revealed that all studied inputs significantly impacted the transformation of DXC.

Keywords: Doxycycline hydrate, Modelling, Photo-Fenton, Optimized Artificial Neural Network, Removal.

HIGHLIGHTS

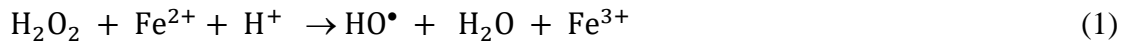
- Hydroxyl radicals transform efficiently doxycycline hyclate from aqueous solution
- Experimental optimisation showing strongly effect of: pH, concentration of DXC, H₂O₂ and Fe²⁺
- Designed OANN present a very good correlation between experimental and predict removal efficiency

Introduction

Currently, the production or even the consumption of antibiotics has become more and more increasing, this has caused their presence continuously in liquid effluents and even in soils either as original or in metabolic forms [1]. It has been reported that tetracycline antibiotics are the second class of antibiotics produced and used throughout the world, they were used mainly in veterinary and human therapy as well as feed additives for animals. However, the existence of tetracycline (TCs) in wastewater can influence the quality of surface water, groundwater, soils, aquaculture, animals, and humans [2]. However, TCs molecules have a typical structure like naphthalene resisting degradation and metabolic reactions, then, they are released into the environment in their original structure. Therefore, exposure to TCs, for example in drinking or irrigation water, can cause potential damage to living organisms and the environment. Moreover, TCs can cause microorganisms to develop resistance to drugs by producing antibiotic-resistance genes and inducing human and animal metabolism [3]. It has been revealed that TCs can reduce the growing functions of teeth and skeleton of fetuses and children thus estrogenic effects [4]. Also, TCs antibiotics pose severe threats to the development and metabolism of plants, by inhibiting biomass accumulation, decreasing pigment content, and increasing reactive oxygen species and antioxidant enzymes [5]. Doxycycline (DXC) in its hyclate form is a semi-synthetic tetracycline molecule, it has a large activity spectrum against Gram-positive and Gram-negative bacteria which is widely used in human and veterinary practice [1,6]. As a result, DXC can be detected as it is in livestock, fish, vegetables, fruits, and in different sources of water, wastewater, and soil [6]. Recently, Advanced Oxidation Processes (AOPs) have generated hydroxyl radicals which are very reactive and no selective oxidant for a great variety of organic compounds. These radicals can be generated from some oxidizing reactants like hydrogen peroxide or ozone combined with the presence of metallic or semiconductor catalysts within or without energy [7].

The PF oxidation, is a metal-catalyzed oxidation reaction occurring in the presence of iron through a chain of radical reactions which allows the generation of hydroxyl radicals (Eq. (1)). In addition, the association of hydrogen peroxide/ferrous ions with UV radiation enhances the efficiency of oxidation process especially the rate of degradation of organic pollutants by additional generation of hydroxyl radicals from different reactions [8].

In the Fenton reaction, ferric ions may accumulate and the reaction and the reaction chain do not continue if the ferrous ions are completely consumed[9]. Thus, ferric ions catalyze the decomposition of hydrogen peroxide (Eqs: (2) and (3))[8].



As shown in Eqs (4) and (5), consumption of hydroxyl radicals may occur which leads to the reduction of Fenton process efficiency [8].



In the presence of UV radiation, HO^\bullet was formed by the reduction of Fe^{3+} into Fe^{2+} (Eq (6)), decomposition of H_2O_2 into two molecules of HO^\bullet (Eq (7)), and photolysis of ferric complexes produced during the reaction chain process (Eq (8)) [7].

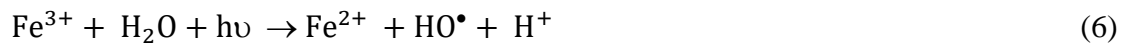


Photo-Fenton process as homogeneous AOPs has been considered a potentially effective process allowing the removal and mineralization of the majority of non-biodegradable and recalcitrant micro-pollutants such as tetracycline molecules [6]. In addition, due to its simplicity, the PF process is recognized by a low cost, fast reaction rate and no amount of sludge can be produced [7]. It has been reported that the oxidative mechanism pathway of DXC by hydroxyl radicals has been proposed by several studies, which can lead to small molecules and/or complete mineralization [1, 6]. Likewise, Fenton oxidation, the number, and complexity of the reactions that can take place during PF oxidation, on the one hand, and since the intervention of several parameters in the efficiency of the elimination process, statistical modeling methods are unable to predict or to simulate effectively oxidation by hydroxyl radicals, Artificial neural network (ANN) methods has attracted attention researchers to simulate, model and predict all type of phenomena in various discipline of sciences and engineering. Many studies proved the capacity and rapidity of these methods to solve numerous problems of environmental engineering, such as the adsorption of organic pollutants[10], membrane separation [11], and biological treatment[12]. Nevertheless, it has been reported that in the last decade, the application of ANN has been increasingly applied in AOPs especially for dye removal [13], but a few researches have been carried out

on the application of ANN in PF processes for the removal of antibiotics compounds [14]. In their work, Talwar et al. [15] and Sethi et.al [16], studied the transformation of different molecules with therapeutic effects such as amoxicillin, and metronidazole by photocatalytic methods which are more expensive and applied modeling based on the combination of several artificial intelligence methods, this and despite the effectiveness of the methodology applied, makes the procedure. However, the application of neural modeling in the present study is since it is simple and rapid and has proven its effectiveness in several areas. in addition, it has not previously been applied to the transformation of the DXC molecule by the photo-Fenton process.

The present work focuses on assessing the effectiveness of the $\text{H}_2\text{O}_2/\text{Fe}^{+2}$ /solar irradiation system to remove doxycycline hyclate from an aqueous solution by experimental and modeling study. To achieve this objective, four variables were targeted: pH, doxycycline, hydrogen peroxide, and catalysis concentration. The performance of the optimized ANN model was conducted by evaluating the predicted in contrast to experimental removal efficiency. Finally, the impact and the importance of each input variable on removal efficiency as the output variable was determined.

Experimental

Materials

Doxycycline hyclate (DXC) was provided by the Antibiotical-Saidal pharmaceutical group (Medea, Algeria). The chemical structure and physico-chemical properties are shown in Table 1. Hydrogen peroxide solution (30%, w/w) and salt of iron in the form of ferrous sulfate heptahydrate ($\text{FeSO}_4 \cdot 7\text{H}_2\text{O}$) were purchased from Sigma-Aldrich Corporation (St. Louis, MO, USA) and all other chemicals were of analytical grade and were used without further purification.

Table 1

Experimental methods

The PF oxidation is a metal-catalyzed oxidation reaction occurring in the presence of iron through a chain of radical reactions which allows the generation of hydroxyl radicals (Eq. (1)). In addition, the association of hydrogen peroxide/ferrous ions with UV radiation enhances the efficiency of oxidation process especially the rate of degradation of organic pollutants by additional generation of hydroxyl radicals from different reactions [8].

Experiments were carried out in a borosilicate reactor (0.1 L) menu with a water jacket maintaining a constant temperature (24 ± 2 °C). The radiation was provided from solar irradiation with light intensity and luminance varying from 450 to 600 W/m² and 95 to 100 klx, respectively. A volume of 50 mL of reaction mixture containing an appropriate concentration of DXC and hydrogen peroxide was illuminated by solar radiation under magnetic stirring. After, ferrous ions (as ferrous sulfate heptahydrate) were added and the mixture was stirred magnetically for a duration of 30 min (Figure 1). The pH effect was investigated by using different buffer solutions: 20 mM potassium chloride/HCl buffer (pH 2 and 2.5), 20 mM potassium phthalate/HCl buffer (pH 3, 3.5 and 4), and 20 mM potassium phthalate/NaOH buffer (pH 4.5 and 5). The parameters taken in this study, on which removal of DXC depends, are pH, initial concentration of DXC, H₂O₂, and Fe²⁺ (Table 2).

In the end, the mixture was centrifuged at 4.000 rpm for 10 min and the supernatant and the precipitates were monitored for spectroscopies, chromatography, and toxicity analysis.

The experiments were conducted in triplicate and their average were reported.

Figure 1

Table 2

Characterization methods

The DXC concentration was determined with a UV-visible spectrophotometer (Model Perkin-Elmer 550 A) at different wavelengths ranging from 200 to 600 nm. The residual DXC concentration after treatment with PF oxidation was evaluated on the supernatant at the maximum wavelength of DXC (375 nm).

The removal efficiency (RE) was calculated as follows (Eq (9)) [17]:

$$RE (\%) = \frac{C_0 - C_t}{C_0} \cdot 100 \quad (9)$$

Where C₀ and C_t (mg/L) are the initial DXC concentration and its concentration at time (t) respectively.

FTIR spectra of dried DXC and its precipitate degradation products have been recorded for the KBr pellet. FTIR spectra were done in the mid-IR region of 400-4000 cm⁻¹ and were collected at the absorbance mode in a Shimadzu 8400 spectrophotometer at 4 cm⁻¹ resolution and a number of scans of 128. A High-Performance Liquid Chromatography (Alliance Waters e2695) equipped with a UV-Visible detector (Waters 2489) operated at 280 nm \pm 4nm, an

automatic sample injector, a 3DR solvent delivery system, a thermostated column compartment adjusted at 60°C and a stationary phase constituted by a Reverse-Phase column (RP18, 4.6mmx25cm), is used to get the elution data of DXC and its extracted degradation products. The elution process was carried out using a mobile phase made up of the reagent cited in Table 3. The flow rate is to 1 mL/min. The injection volume was 20 µL which was conducted with an automatic injector.

Table 3

Artificial neural network modeling

Artificial neural networks (ANN) are mathematical models, which have similar principles and share basic elements with the nervous system to take actions based on perception rather than reasoning. Modeling consists of implementing a system of neural networks in an artificial mode, to set correspondence for each composing the biological neuron (Figure 2).

Figure 2

In the present study, the adopted methodology for the removal efficiency prediction of DXC by the neuronal technique can be summarized into four steps: selection of neural model inputs, data collection, data division sets, and data normalization. The input variables for the feed-forward neural network are pH, initial DXC concentration (mg/L), initial H₂O₂ concentration (mg/L), and initial Fe⁺² concentration. The output variable selected was removal efficiency. Table 4 contains the statistical analysis of the inputs and output data which are expressed by minimum, mean, maximum, and standard deviation.

Table 4

The total experimental database was divided into three subsets: training (67%), testing (17%), and validation (16%). Since there is a difference within the input data ranges, a normalization is essential, all input and output data were converted into normalized values in the -1 and +1 range using Eq. (10) expressed as follows:

$$y_n = \frac{2*(y-y_{min})}{(y_{max}-y_{min})} - 1 \quad (10)$$

Where y_n is the input or output variable y , and y_{min} and y_{max} are the minimum and maximum values of variable y , respectively.

Figure 3 details the design principle of the ANN model in this study.

To optimize the topology of the network architecture, it was necessary to determine the optimum number of hidden neurons, in which some statistical parameters such as R^2 , MSE, RMSE, and MAE, could calculate for the training process.

Figure 3

Results and discussion

Effect of pH, CTC, Hydrogen peroxide, and ferrous ions doses

It has been demonstrated that common operating parameters affecting efficiency removal in terms of quality and quantity in all Fenton processes are: pH, organics, oxidant, and catalysis concentrations [7]. The pH of the reaction medium affects strongly the production of hydroxyl radicals. However, the photolysis process of hydrogen peroxide is independent of the pH condition. Therefore, it has been reported that PF oxidation can remove organic pollutants in neutral and acidic mediums [8]. Therefore, according to Figure 4, at high acidity ($\text{pH} < 3$), the removal efficiency of DXC is very low (about 40%), this can be explained by the slowing down of the Fenton reaction due to the stability of hydrogen peroxide at acidic pH which reacts with protons to form oxonium ions (Eq. 11). Moreover, the excess of H^+ could acting as scavenger of hydroxyl radicals as shown in Eq.12 [8].



Therefore, at low acidity ($\text{pH} \geq 4$), the process of photo-oxidation using ferrous ions favors the formation of hydroxyl ions as hydroxyl radicals (Eq.13) which precipitate with iron ions under complex species. Also, the auto decomposition of hydrogen peroxide is accelerated at higher pH, this must reduce the activity of the Fenton reagent [18].



At pH equal to 3, it was observed that the maximum of the RE of DXC was achieved (67.074%), for which the hydroxy-ferric complexes are more soluble and the $\text{Fe}(\text{OH})^{2+}$ ions are more photoactive [18]. Therefore, another chief systematic parameter assessing the performance of FPs treatment is the micropollutant concentration in the contaminated effluent. The influence of this parameter was studied for DXC ranging from 0.5 to 6.5 mg/L, at pH 3 and for doses of H_2O_2 and Fe^{2+} of 60.0245 mg/L and 86.8 mg/L, respectively. It is shown in Figure 4 that an oxidation potential was observed under these conditions. Nevertheless, the curve allure shows clearly that for DXC concentrations varying from 0.5 to 2.5 mg/L, Whereas, it has been reported that removal efficiency by PF oxidation, increases

with an increase in H₂O₂ dose until optimum concentration [8]. However, results depicted in Figure 4 showed that from a concentration of H₂O₂ of 76.53 mg/L up to 110.54 mg/L, the RE decreases slightly. First, the amount of H₂O₂ was consumed following the ratios of Fe²⁺/H₂O₂ and H₂O₂/UV reactions. This led to the remarkable removal of organic pollutants by the hydroxyl radicals thus formed. Therefore, as reported in the literature, in the PF process, the excessive H₂O₂ improves the scavenging of HO[•] which strongly reduces removal efficiency [7]. In our case, this phenomenon was limited by the photolysis reaction of hydrogen peroxide. Also, regarding Figure 3, the results indicate that the DXC removal has a slower character without ferrous dosage (i.e) H₂O₂/UV process (RE = 17.87%), whereas, the PF process occurs rather faster for ferrous doses of 2.8 mg/L (RE = 43.22%). Moreover, since the ferrous dosages increase from 2.8 to 36.54mg/L, the RE achieves 70.95% which is due to the increasing generation of hydroxyl radicals from the Fenton reaction plus the chemical reduction of hydroxyl-ferric. It has been reported that an increase in ferrous dosage in PF oxidation changes the final pH of the solution from 3.5 to 4.4, thus leading to the formation of iron oxyhydroxide which precipitates and then reduces penetration of light throughout the solution [19].

UV-visible spectra, FTIR, and HPLC analysis of the CTC treated by PF process

As indicated in Figure 5-a, the spectrum of DXC contains three main absorption bands, two were located in the UV region at 245 and 275 nm, and the third in the visible region at 375 nm. For the treated solution spectrum, it was shown that the three absorption bands were strongly reduced after PF treatment. This suggests that the chromophore and the auxochrome groups were converted as well as related auxochrome groups to an aromatic ring [20]. this is likely due to the formation of new aromatic intermediates or other products. 15, 43. however, since •OH is involved in a non-selective reaction by acting on the breakdown of functional groups and hydroxylation of the aromatic structure of tetracyclines, which consequently results in the formation of smaller organic molecules [21]. Pulicharla et al. [21] proposed a reaction mechanism of chlortetracycline (TCs molecule) by Fenton oxidation. They suggested that hydroxyl radicals are disposed to act on carbon-dimethyl amino and carbon-carboxyl amide groups.

Figure 4

Figure 5

As a result, the formation of tricyclic and bicyclic aromatic intermediate compounds leads to smaller organic molecules. Hence, Bolobajev et al. [6] have depicted a complete mineralization of DXC by auto-degradation involving $\text{Fe}^{3+}/\text{H}_2\text{O}_2/\text{UV-C}$ which is very promising by reduction of ferric ions to ferrous ions as well as DXC- Fe^{3+} complex formation leading to a reductive release of Fe(II) while ensuring the generation of HO^\bullet by photolysis and photo-reduction.

Besides, as shown in Figure 5-b, for FTIR spectra of the original DXC sample and its degradation products, the transformation of the parent molecule by PF oxidation was achieved. The FTIR spectrum of the metabolite product as precipitate showed a significant reduction in the number and band absorption compared to the untreated molecule spectrum. The absence of the different characteristics of stretching bands confirms that the functional groups may be transformed by hydroxyl radicals. New position bands of $-\text{C}=\text{C}-$ of the aromatic ring group appeared at 1450 and 1550 cm^{-1} , this may be due to a bathochromic effect of new substituted groups. In addition, a transformation of DXC by hydroxyl radicals generated by PF reaction was performed by its HPLC chromatograms. The chromatogram of the DXC original solution (Figure 6-a) revealed a single peak having a retention time equal to 22.15 min. Nevertheless, the disappearance of the peak corresponding to the DXC molecule can be seen in the chromatogram of extracted degradation products (Figure 6-b), whereas a new peak takes place at a retention time equal to 4.941min. This must confirm the transformation of functional polar groups of DXC molecules by hydroxyl radicals as well as the formation of new molecules.

Figure 6

ANN modeling

To obtain the best combination of components for an ANN-MLP architecture for the prediction of removal efficiency of DXC by PF process, three-layered have been used: input layer, one hidden layer using tangent sigmoid (*tansig*) function as a transfer function, and output layer using linear (*purelin*) function as transfer function (Figure S1). From Table S1, it was observed that the suitable network architecture was taken for 18 neurons in the hidden layer with 150000 iterations.

Figure S1

Table S1

The dispersed diagrams are revealed in Figure S2. It has been observed that the plotting of the predicted RE using experimental results is very satisfactory. The values of MSE and R^2 for the training phase were found to be $2.9759 \cdot 10^{-5}$ and 0.99998, respectively, which indicated that the predicted outputs were very agreed with the corresponding experimental. For the phases of testing and validation, it also indicated that the developed neural model reproduces effectively all used data.

Figure S2

The structure of the model which gives the lowest MSE consists of one hidden layer (*tansig*) with 18 neurons and (*purelin*) as a transfer function at the output layer. The developed model showed an excellent performance with a determination coefficient (R^2) of 0.997 and MSE of $3.76 \cdot 10^{-4}$. Elmolla et al. [22] have developed an ANN model to predict the performance of FP for the removal of amoxicillin, ampicillin, and cloxacillin. The configuration of the backpropagation neural network giving the smallest mean square error (MSE) was a three-layer ANN with tangent sigmoid transfer function (*tansig*) at hidden layer with 14 neurons, linear transfer function (*purelin*) at the output layer and Levenberg–Marquardt backpropagation training algorithm (LMA) with a determination coefficient (R^2) of 0.997 and MSE of $3.76 \cdot 10^{-4}$.

Global sensitivity analysis

In the present study, the weight method was carried out to perform the effect of each input variable on the output variable: an equation using a partitioning of connection weights (Eq. 14) can be used, [23]:

$$I_j = \frac{\sum_{m=1}^{m=N_h} \left(\frac{|(w_{jm}^{ih})|}{\sum_{k=1}^{N_i} |w_{km}^{ih}|} \right) * \text{abs}(W_{mn}^{ho})}{\sum_{k=1}^{N_i} \left(\sum_{m=1}^{m=N_h} \left(\frac{|(w_{km}^{ih})|}{\sum_{k=1}^{N_i} |w_{km}^{ih}|} \right) * |(W_{mn}^{ho})| \right)} \quad (14)$$

Where I_j is the relative sensitivity of the j^{th} input variable to the output parameter; N_i and N_h represent the number of input and hidden neurons, respectively; "W" are connection weights. The exponent i, h and o refer to the input, hidden, and output layers, respectively, and the clues k, m and n refer to the input, hidden, and output layers, respectively.

As indicated in Figure S3, all variables have strong effects on the removal efficiency of DXC. Therefore, initial DXC and catalysis concentrations were depicted to be the significant influential parameter with a relative influence of 27% then pH (24%), as well as hydrogen peroxide initial dosage (22%). Some anterior research carried out on the removal of organic

molecules by the PF process reported different values of the relative importance of input variables, this may depend on operational conditions and variables that the researcher has taken into account [21,23,24].

Figure S3

To facilitate the computing of the output variable (RE) knowing only the selected inputs (pH, [DXC]₀, [H₂O₂]₀, and [Fe²⁺]₀) through the best-established ANN architecture (weights and biases), a graphical interface (Figure S4) was developed via a MATLAB program.

Figure S4

Conclusion

The removal efficiency of doxycycline hyclate by homogeneous photocatalysis H₂O₂/Fe²⁺/UV reached a maximum value of 79% at pH 3, 2.5 mg/L of DXC, 76.5315 mg/L of H₂O₂ and 86.8 mg/L of Fe²⁺. Spectroscopy and chromatography analysis confirmed the potential capacity of the photo-Fenton process to transform doxycycline molecule on small fragment metabolite. Therefore, a three-layered feed-forward back propagation ANN was developed to predict removal efficiency using experimental data. The structure of the OANN-MLP that yielded the best statistical parameters: MSE equal to 2.9759.10⁻⁵ and R² equal to 0.99998, consisted of one hidden layer with a *tansig* function using 18 neurons and *purelin* function as the output layer function. Sensitivity analysis showed that initial concentrations of doxycycline and ferrous ions have the most effect on removal efficiency (27%). Finally, the results of interpolation and extrapolation confirmed that the ANN model could effectively reproduce experimental data and predict the performance of the process in the domain of the studied input variables.

Acknowledgment

The authors are grateful to the Laboratory of BioMaterial and Transport Phenomena (LBMTTP) for the provided help and encouragement. The authors also thank Pr. Bouaziz M.N, University of MEDEA for his immense contribution.

Graphical abstract

References

- [1] A. A. Borghi, M. F. Silva, S. Al Arni, A. Converti, and M. S. A. Palma, *J. Chem.* 2015 (2015) 1-9. <https://doi.org/10.1155/2015/492030>
- [2] D. Xu Y. Gao, Z. Lin, W. Gao, H. Zhang, K. Karnowo, X. Hu, H. Sun, S. Shatir, S. Hassan, S. Zhang, *Front. Chem.* 7 (2020) 1-18. <https://doi.org/10.3389/fchem.2019.00943>
- [3] J. Scaria, K. V. Anupama, and P. V. Nidheesh, *Sci. Total Environ.* 771 (2021) 145291. <https://doi.org/10.1016/j.scitotenv.2021.145291>
- [4] R. Daghrir and P. Drogui, *Environ. Chem. Lett.* 11 (2013) 151-156. <https://doi.org/10.1007/s10311-012-0390-2>
- [5] T. Han, Y. Liang, Z. Wu, L. Zhang, Z. Liu, Q. Li, X. Chen, W. Guo, L. Jiang, F. Pan, S. Ge, Z. Mi, Z. Liu, H. Huang, X. Li, J. Zhou, Y. Li, J. Wang, Z. Zhang, Y. Tang, M. Wu, *J. Hazard. Mater.* 380 (2019) 120885. <https://doi.org/10.1016/j.jhazmat.2019.120885>
- [6] J. Bolobajev, M. Trapido, and A. Goi, *Chemosphere* 153 (2016) 20-23. <http://doi.org/10.1016/j.chemosphere.2016.03.042>
- [7] M. hui Zhang, H. Dong, L. Zhao, D. xi Wang, and D. Meng, *Sci. Total Environ.* 670 (2019) 11-21. <https://doi.org/10.1016/j.scitotenv.2019.03.180>
- [8] P. V. Nidheesh, R. Gandhimathi, and S. T. Ramesh, *Environ. Sci. Pollut. Res.* 20 (2013) 2099–2132. <https://doi.org/10.1007/s11356-012-1385-z>
- [9] S. M. Aramyan, *Int. J. Environ. Sci. Nat. Resour.* 2 (2017) 1-18. ISSN: 2572-1119
- [10] Y. Mesellem, A. A. El Hadj, M. Laidi, S. Hanini, and M. Hentabli, *Neural Comput. Appl* 2 (2021). <https://doi.org/10.1007/s00521-021-05890-2>
- [11] A. Adda, S. Hanini, S. Bezari, M. Laidi, and M. Abbas, *Environ. Eng. Res.* 27 (2021). <https://doi.org/10.4491/eer.2020.383>
- [12] P. Kundu, A. Debsarkar, S. Mukherjee, and S. Kumar, *Environ. Technol. (United Kingdom)*. 35 (2014) 1296-1306. <https://doi.org/10.1080/09593330.2013.866698>
- [13] A. Giwa, A. Yusuf, H.A. Balogun, N.S. Sambudi, M.R. Bilad, I. Adeyemi, S. Chakraborty, S. Curcio, *Process Saf. Environ. Prot.* 146 (2021) 220-256. <https://doi.org/10.1016/j.psep.2020.08.015>
- [14] O. B. Ayodele, H. S. Auta, and N. Md Nor, *Ind. Eng. Chem. Res.* 51 (2012) 1611-1619. <https://doi.org/10.1021/ie302390b>

- [15] S. Talwar, A. K. Verma, and V. K. Sangal, *J. Environ. Manage.*, 250, no. July, (2019), doi: 10.1016/j.jenvman.2019.109428.
- [16] S. Sethi, A. Dhir, and V. Arora, *React. Kinet. Mech. Catal.*, 136, no. 1, (2023) 549–565, doi: 10.1007/s11144-023-02360-9
- [17] N. Boucherit, M. Abouseoud, and L. Adour, *Nov. Biotechnol. Chim.* 17 (2018) 160–171. <https://doi.org/10.2478/nbec-2018-0017>
- [18] A. Babuponnusami and K. Muthukumar, *J. Environ. Chem. Eng.* 2 (2014) 220-226. <http://doi.org/10.1016/j.jece.2013.10.011>
- [19] L.G. Devi, K.E. Rajashekhar, K.S. Anantha Raju, S.G. Kumar, *Desalination* 270 (2011) 31-39. <http://doi.org/10.1016/j.desal.2010.11.017> [20] J. Jeong, W. Song, W. J. Cooper, J. Jung, and J. Greaves, *Chemosphere* 78 (2010) 535-540. <http://doi.org/10.1016/j.chemosphere.2009.11.024>
- [21] R. Pulicharla S.K. Brar, T. Rouissi, S. Auger, P. Drogui, M. Verma, R.Y. Surampalli, *Ultrason. Sonochem.* 34 (2017) 332-342. <http://doi.org/10.1016/j.ultsonch.2016.05.042>
- [22] E. S. Elmolla, M. Chaudhuri, and M. M. Eltoukhy, , *J. Hazard. Mater.* 179 (2010) 127-134. <http://doi.org/10.1016/j.jhazmat.2010.02.068>
- [23] M. Laidi and S. Hanini, *Int. J. Refrig.* 36 (2013) 247-257. <http://doi.org/10.1016/j.ijrefrig.2012.09.016>

List of symbols and abbreviations

ANN: Artificial Neuronal Network

AOP: Advanced Oxidation Process

C_0 : Initial DXC concentration, mg/L

C_t : DXC concentration at a time t , mg/L

DXC: Doxycycline hyclate

FTIR: Fourier Transform Infrared

HPLC: High-Performance Liquid Chromatography

I_j : Relative sensitivity of the j^{th} input variable to the output parameter

M_i : Molecular weight of each molecule, such as doxycycline hyclate, hydrogen peroxide, and iron

MAE: Absolute mean error

MSE: Mean squared error

NRMSE: Root of the normalized mean squared error

N_i and N_h : Number of neurons in the input and hidden layers, respectively

PF: Photo-Fenton

RE: Removal efficiency, %

TC: Tetracycline

RMSE: Root mean squared error

R^2 : Coefficient of determination

y_{norm} : Normalized value

y : Experimental data

y_{max} : Maximum experimental value

y_{min} : Minimum experimental value

W : Connection weights

Figure captions:

Figure 1 Schematic representation of photo-Fenton reaction of DXC

Figure 2 Schematic representation of the similarity between biological neuron and an ANN

Figure 3 Architecture of the ANN-MLP model

Figure 4 Effect of pH and concentration of DXC, H₂O₂ and Fe²⁺ on RE by PFP.

Figure 5 (I) UV-visible spectra of CTC before and after photo-Fenton treatment, and (II) FTIR of a) CTC, and b) its transformed products

Figure 6 HPLC chromatograms of DXC aqueous solution before PF treatment a) and after PF treatment b)

Table 1. Physicochemical properties of doxycycline hyclate.

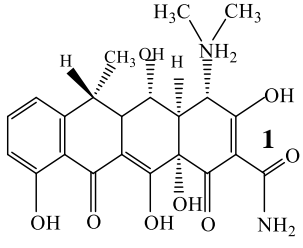
Chemical structure	Characteristic	Value
	Molecular Weight (g/mol)	1025.87
	Water solubility (293°K, mg/mL)	50
	Appearance	yellow crystalline
	Purity (%)	98.5
	λ_{\max} (nm)	375
	$pK_{a1}^{a2,a3}$	7.07, 9.13
		3.50

Table 2. Variables and their levels

Level	pH	[DXC] ₀	[H ₂ O ₂] ₀	[Fe ²⁺] ₀
1	2	0.50	8.5035	2.8
2	2.5	1.50	25.510	19.6
3	3	2.50	42.517	36.4
4	3.5	3.50	60.024	53.2
5	4	4.50	76.531	70
6	4.5	5.50	93.538	86.8
7	5	6.50	110.54	103.6

Table 3. Mobile phase composition

Reagent	Monobasic phosphate potassium	Sodium hydroxide	Tetrabutyl-ammonium-hydrogen sulfate	Edetate disodium	Tertiary butyl alcohol
	2.72 g	0.74 g	0.50 g	0.40 g	60 g

Table 4. Statistical analysis of inputs and output data

	Min	Mean	Max	STD
pH	2	3.0637	5	0.3256
[DXC] ₀ (mg/L)	0.5000	2.7614	6.5000	1.0219
[H ₂ O ₂] ₀ (mg/L)	8.5161	61.1409	110.8700	23.2844
[Fe ²⁺] ₀ (mg/L)	2.7814	67.0639	103.9130	29.4269
RE (%)	9.7435	63.7960	80.2030	13.2515

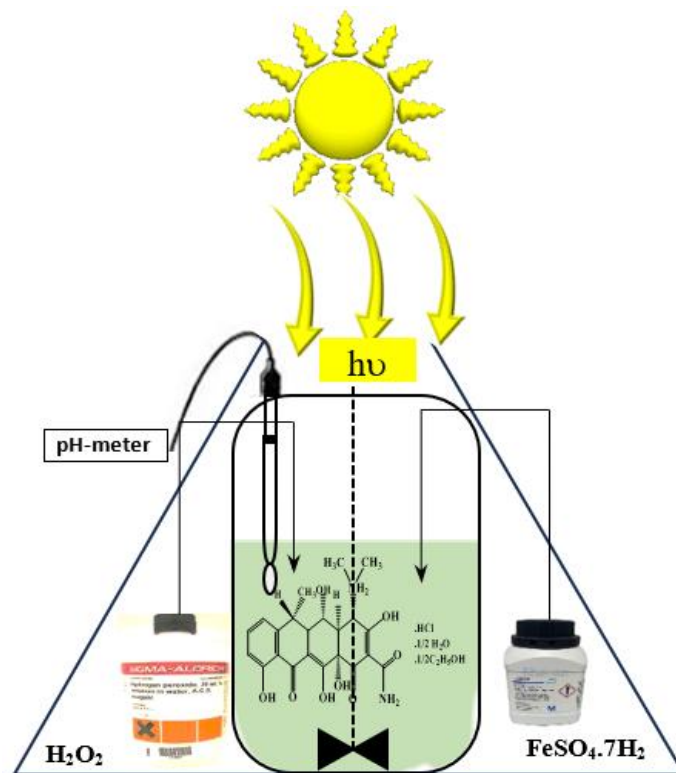


Figure 1

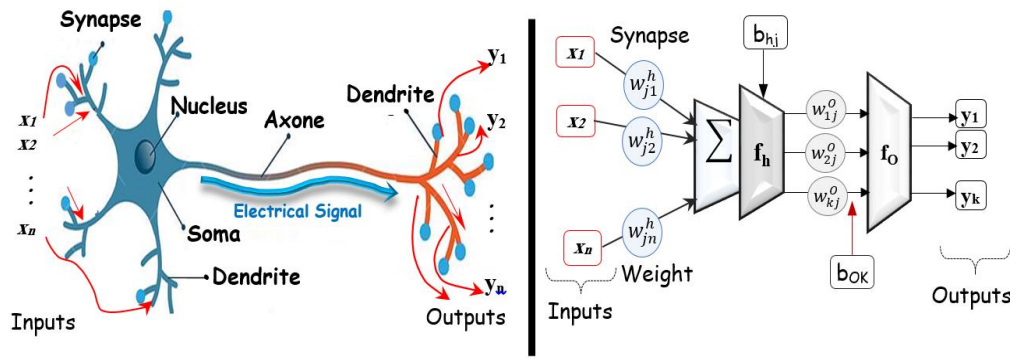


Figure 2

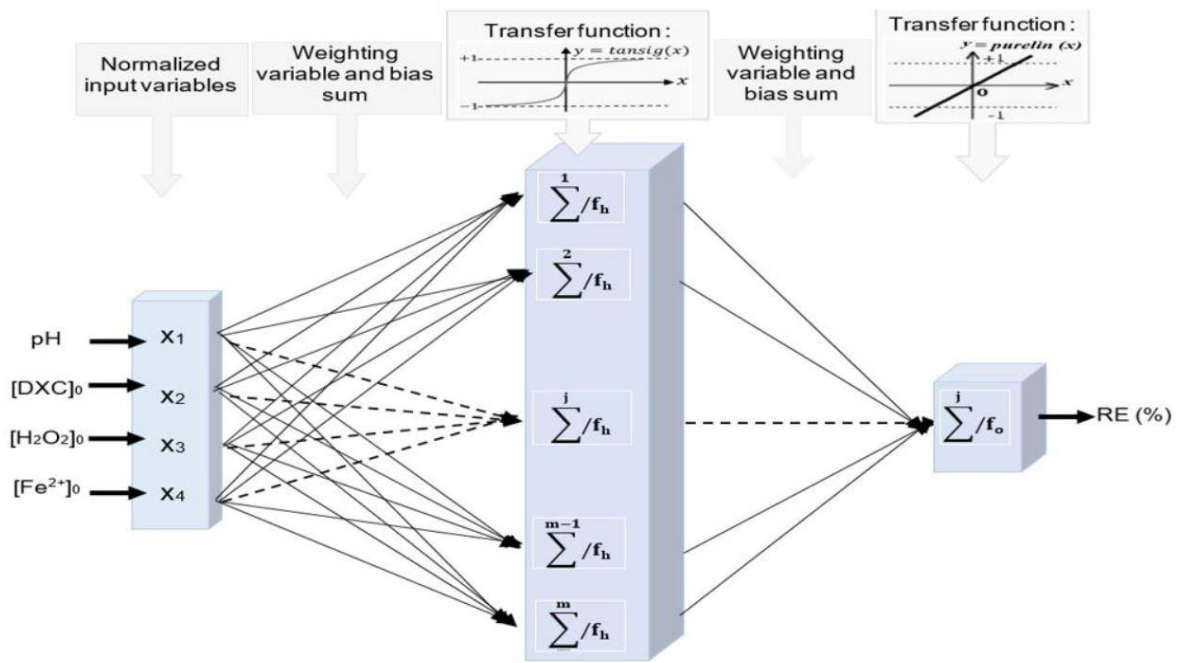


Figure 3

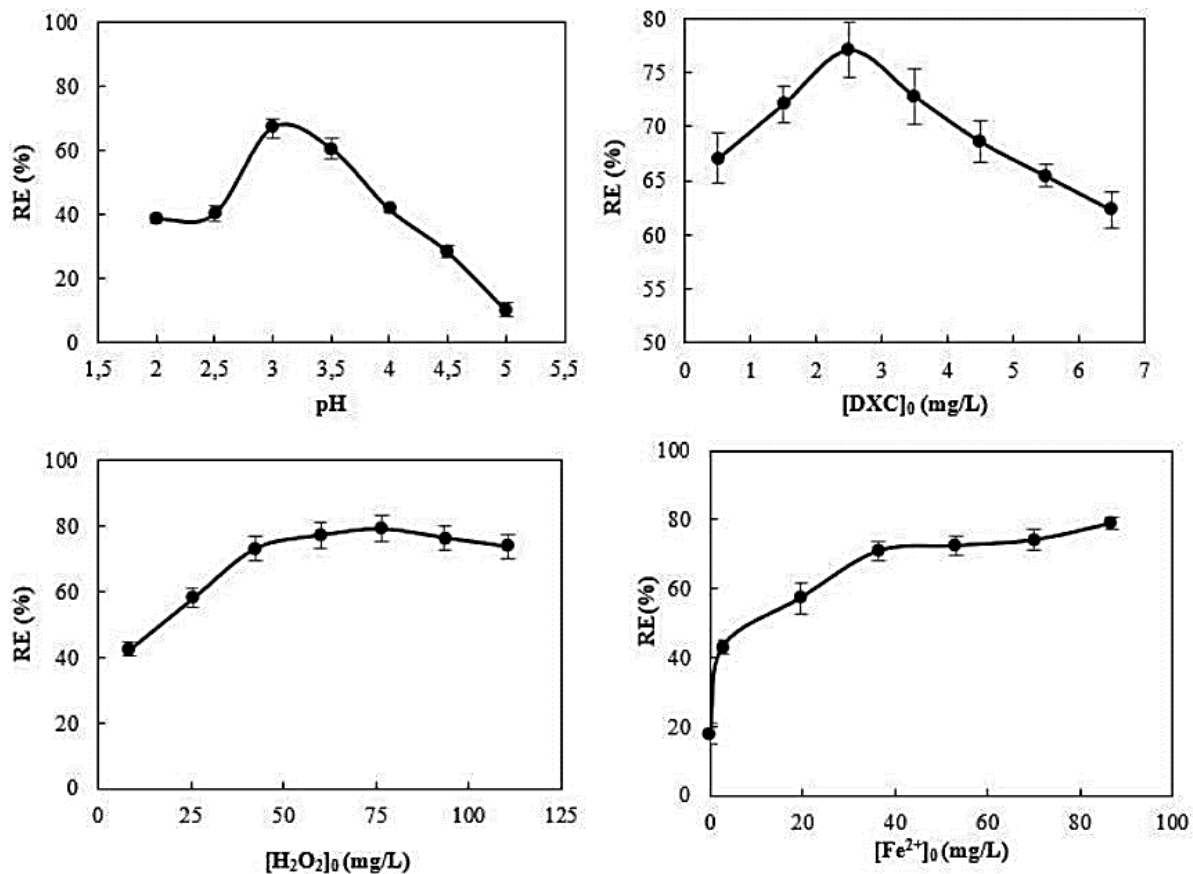


Figure 4

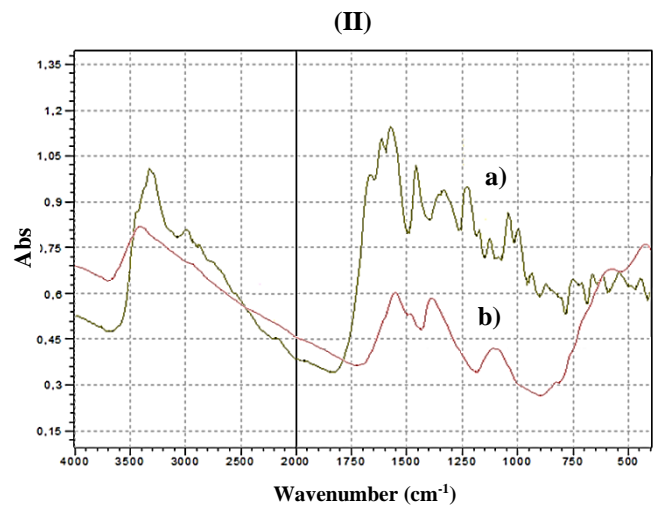
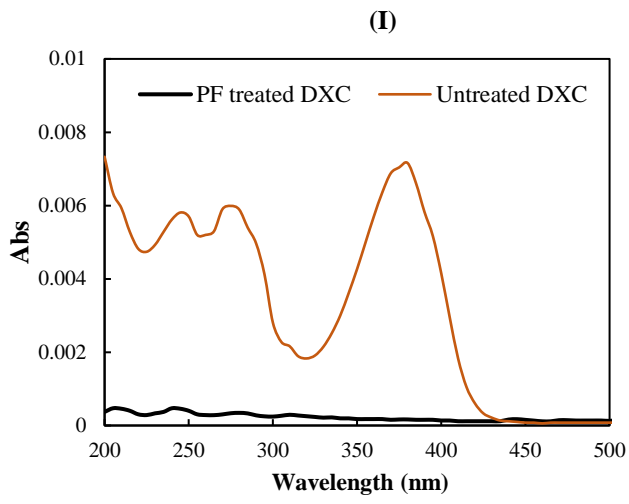


Figure 5

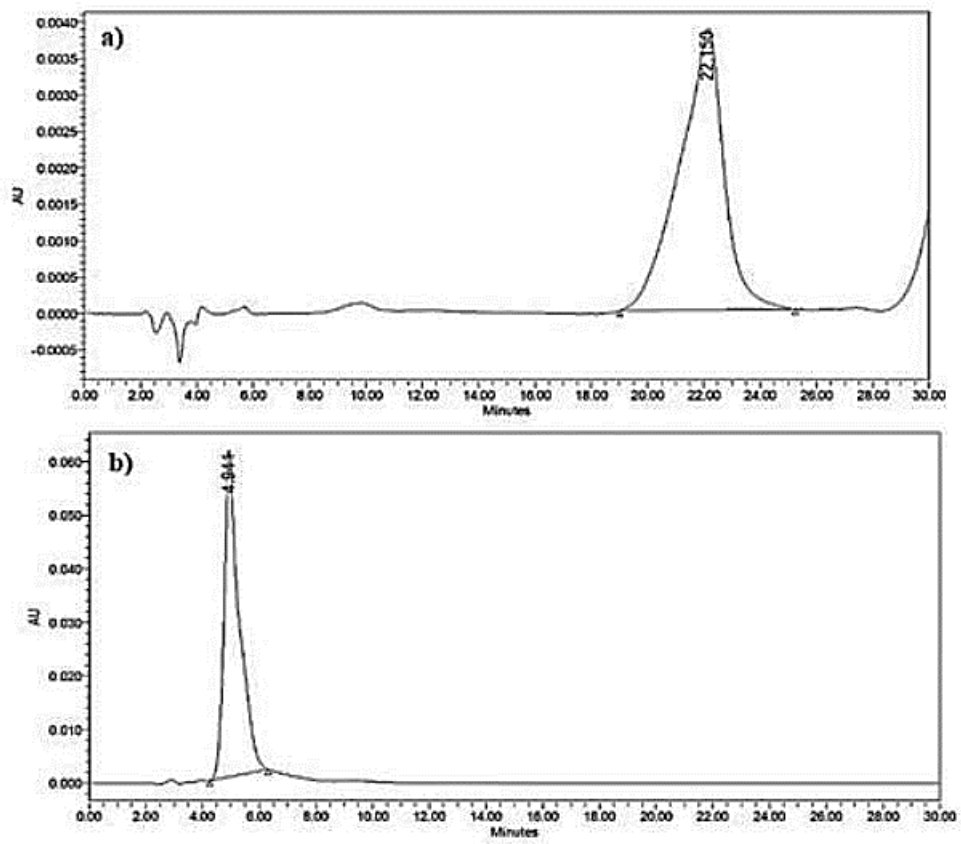


Figure 6